Adaptive phase estimation filter in long range synthetic aperture sonar interferometry

Torstein Olsmo Sæbø[1,✉] and Roy Edgar Hansen[1,2]
[1]Norwegian Defence Research Establishment (FFI), Kjeller, Norway
[2]Department of Informatics, University of Oslo, Oslo, Norway
✉ E-mail: torstein-olsmo.sabo@ffi.no

Synthetic aperture sonar (SAS) interferometry is a technique for very high resolution imaging and mapping of the seabed. In SAS interferometry, the seabed depth estimation performance is a function of the system, the geometry, the signal-to-noise ratio (SNR) and the filter size, equivalent to the achieved horizontal resolution. A strong driver for SNR is the imaging range and grazing angle. The variation of these parameters over a typical SAS swath gives rise to a large variation in the depth estimation performance. To mitigate the negative effect of this, we suggest to use an adaptive phase estimation filter size, such that the standard deviation of the depth estimate is proportional to the horizontal resolution. We demonstrate the suggested adaptive filter size method on long range data collected using a HUGIN Superior autonomous underwater vehicle (AUV) equipped with a HISAS 1032 Dual receiver interferometric SAS. Our technique increases the valid area coverage when the SNR is marginal, at the expense of reduced horizontal resolution.

Introduction: Synthetic aperture sonar (SAS) [1] is today considered the reference technique for very high resolution imaging of the seabed. Similar to its counterpart synthetic aperture radar (SAR) [2], SAS provides range independent along-track resolution by coherent combination of multiple pulses in order to synthesize larger apertures. Interferometric SAS [3] is based on using two or more vertically separated receiver arrays such that the vertical direction of arrival, and thereby the depth of the seabed can be estimated. As with SAR interferometry [4], the performance of SAS interferometry is a function of the system, the geometry, the backscattered signal-to-noise ratio (SNR), and the filter size (or correlation window size). The depth estimation accuracy can be divided into a standard deviation (STD) part, and a probability of wrap error part. In difference to SAR interferometry, many interferometric SAS systems are wideband, which again allows for a simpler approach in the phase unwrapping part of the SAS interferometry processing [5]. A challenge in SAS interferometry is the strong geometry induced variation of backscattering signal strength and thereby significant SNR variation in the desired imaging swath [6].

In this paper, we suggest to use an adaptive filter size in the seabed depth estimation such that the estimated STD is proportional to the horizontal resolution, and that the filter size varies with range only. Related techniques have been suggested in multibeam echosounder (MBES) mapping [7] and SAR interferometry mapping [8, 9]. We demonstrate the adaptive filter size method on long range data collected with a HUGIN Superior autonomous underwater vehicle (AUV) equipped with a HISAS 1032 Dual receiver interferometric SAS [10]. Our adaptive filtering increases the valid mapping area coverage compared to a fixed filter size when the SNR is marginal, but at the expense of reduced horizontal resolution.

Background: The common configuration of a SAS system is using an AUV as the host platform, and a starboard and a port SAS system with a nadir gap. The vehicle altitude is chosen such that the sonar swath on the seabed is as large as possible. This gives a relatively horizontal imaging geometry per side (see Figure 1). Such an imaging geometry gives a large spread in sonar range, r, and grazing angle, ϕ_g. These parameters, in addition to the vertical beampattern of the transmitter and receiver, strongly affects the backscattered signal strength, and thereby the SNR [11, 12].

In order to get a better understanding of the SNR dependence of the imaging geometry, we have done a theoretical power budget calculation. We have modelled the backscattering coefficient using the small-slope approximation for elastic roughness scattering, and perturbation theory for elastic volume scattering [13]. We use that together with the sonar/radar equation to calculate the SNR as function of imaging geometry, system settings, and seabed type. The backscattering coefficient calculations here are based on code from Darrel Jackson from Applied Physics Laboratory, University of Washington, USA. The modelled SNR for four different seabed types is shown in Figure 2. We have tuned the transmit power and noise level such that Coarse Sand at maximum range gives comparable results with the experimental data (shown in the next sections). We see that the SNR varies with more than 40 dB over the desired ground range interval for some of the seabed types. For a fixed filter size filtering this will result in very large variations in the STD of the depth estimate.

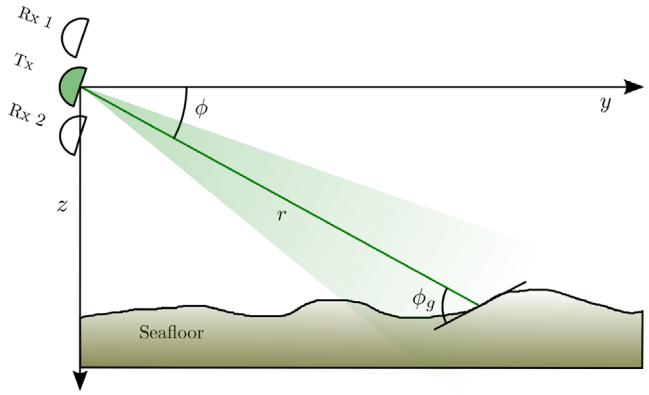

Fig. 1 *Seabed backscattering geometry for a vertical SAS system. Here y is along ground range, z the depth, r the range, ϕ the depression angle, and ϕ_g the grazing angle*

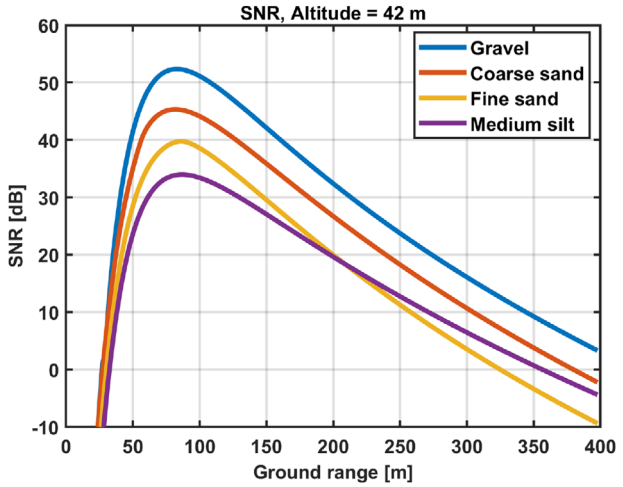

Fig. 2 *Theoretical SNR as a function of ground range for 42 m altitude and four different seabed types*

Method: Consider an interferometric SAS image pair, with along-track grid resolution dx and across-track ground range grid resolution dy. An interferometric estimate can be found by using a moving estimation filter, e.g. a moving complex cross-correlation, of size $M_x \cdot M_y$ pixels on the image pair [5, 14]. Both the grid resolutions and the filter sizes may vary independently, but in this paper we have chosen to keep them both square, i.e. $\mathrm{d}x = \mathrm{d}y \equiv \mathrm{d}\xi$ and $M_x = M_y \equiv M$.

The number of independent samples in the filter (or correlation window), N, is an essential performance parameter. In practice, SAS images are almost always oversampled by a small factor, $\alpha < 1$, such that

$$N = \alpha M^2, \quad \alpha = \frac{\mathrm{d}x}{\mathrm{d}x^{3\mathrm{dB}}} \frac{\mathrm{d}y}{\mathrm{d}y^{3\mathrm{dB}}} \tag{1}$$

Here $\mathrm{d}x^{3\mathrm{dB}}$ and $\mathrm{d}y^{3\mathrm{dB}}$ are the 3 dB resolutions of the complex interferogram, where we also have accounted for the broadening of the resolutions when the SAS images are multiplied together in the interferometric processing and the wavenumber support differs from a square window

[15]. The horizontal resolutions of the interferometric estimate, δx and δy, are simply the size of the estimation filter. This is equal to the grid resolution, $\mathrm{d}\xi$, times the number of pixels on one edge of the filter, M

$$\delta x = \delta y = M\mathrm{d}\xi \tag{2}$$

The theoretical lower bound for the standard deviation of the depth estimate, σ_z, when omitting wrap errors, is given by the square root of the Cramér–Rao lower bound (CRLB) of the time delay estimate [15, 16]

$$\sigma_z \approx \frac{\mathrm{rc}}{D}\frac{1}{2\pi f_\mathrm{c}}\frac{1}{\sqrt{N}}\sqrt{\frac{1}{\rho}+\frac{1}{2\rho^2}} \tag{3}$$

where r is slant range, c the speed of sound, D the vertical baseline, f_c the center frequency and ρ the SNR. Note that this expression assumes vertical interferometer baseline. The SNR, ρ, can be estimated from the correlation coefficient or the interferometric coherence, μ [16, 17]

$$\rho = \frac{\mu}{1-\mu} \tag{4}$$

A standard approach in interferometric processing is to use a fixed filter size, which means that the number of independent pixels in the correlation is $N_\mathrm{fixed} = \alpha M^2$, where M in this case is a constant integer. This is a sensible choice in spaceborne SAR, where the grazing angle and the SNR changes relatively little in the imaging geometry [4, Ch. 2.3]. However, in typical SAS imaging geometries, this approach will lead to large STD at long ranges. Another option is to vary the estimator size, while maintaining a constant theoretical STD of the depth estimate [7]. Since the coherence and thus the SNR is independent of estimator size (ignoring the estimator bias [17]), solving Equation (3) for N gives us

$$N_\mathrm{crlb} = \left(\frac{rc}{D}\frac{1}{2\pi f_\mathrm{c}}\frac{1}{\sigma_z}\right)^2\left(\frac{1}{\rho}+\frac{1}{2\rho^2}\right) \tag{5}$$

Since N_crlb is approximately proportional to r^2/ρ^2 for low SNR, $\rho \ll 1$, M is in this case proportional to r/ρ. This will lead to large estimation windows at long ranges, where the SNR drops rapidly with range.

In this paper, we suggest an alternative solution where adaptive filtering ensures a pre-defined relation between the STD of the depth estimate and the horizontal resolutions. As such, we optimize estimation of 3D-positions of the seabed, instead of only estimation of depth. We define a new criteria

$$\delta x = \delta y \overset{\mathrm{def}}{=} \kappa\sigma_z, \tag{6}$$

where κ is a user-selected scaling parameter, which determines the relation between the horizontal resolutions and the theoretical STD. By setting the right-hand side of Equation (2) equal to the right-hand side of Equation (6), and substituting for M and σ_z using Equations (1) and (3), we get a new expression for N

$$N_\mathrm{adapt} = \frac{\kappa\sqrt{\alpha}}{\mathrm{d}\xi}\frac{\mathrm{rc}}{D}\frac{1}{2\pi f_\mathrm{c}}\sqrt{\frac{1}{\rho}+\frac{1}{2\rho^2}} \tag{7}$$

We see that N_adapt is approximately proportional to r/ρ for low SNR, which means that the number of pixels in each dimension of the estimation filter, M, is proportional to $\sqrt{r/\rho}$. This is a more moderate increase of the filter size for long ranges, than choosing fixed σ_z.

For interferometric processing using fixed filter size, it is often appropriate to only use the estimates where the coherence is above some threshold. This is a simple way to discard estimates with potentially large error. This approach is, however, unfit for an adaptive filter, where the increase in filter size to some extent compensates for the drop in coherence. A better approach is then to threshold on the predicted theoretical STD of the depth estimate.

Results: To evaluate the performance of our suggested adaptive filter we have selected long range SAS data from a HISAS 1032 Dual receiver system [10]. The system has an interferometric baseline $D = 30$ cm and a center frequency $f_\mathrm{c} = 122$ kHz. All data in this paper are processed with $\mathrm{d}\xi = 2$ cm, $\alpha = 0.4$, and $\kappa = 2$. We have chosen a default filter size of 9×9 pixels, and are omitting thresholding the estimates on coherence or STD in our analysis.

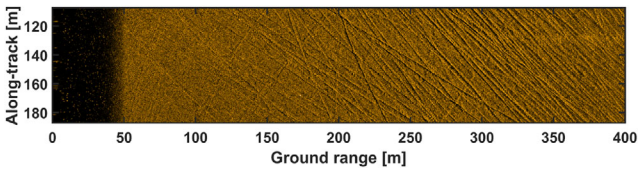

Fig. 3 *SAS image intensity of a 80 m × 400 m flat scene with trawl marks, showing 40 dB dynamic range*

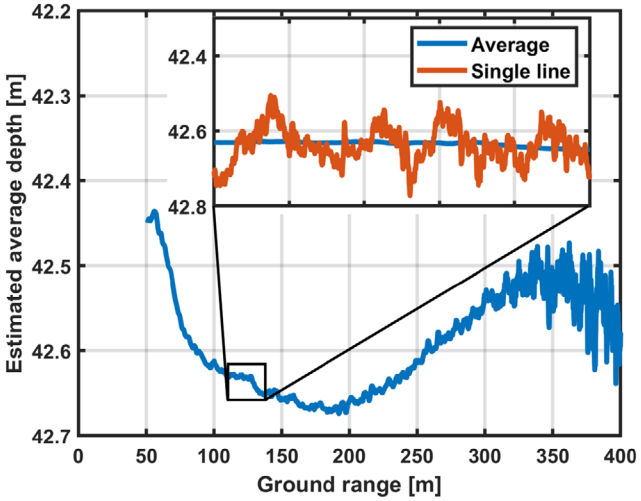

Fig. 4 *Estimated average depth using all along-track measurements and a 1 m sliding window in ground range. Inset panel: Zoom of a 25 m section. Here the corresponding depth estimate for a single ground range line is also included in red. Notice that the* y*-axis differ in the two plots, so the drawn box in the main panel is not the same as the actual inset zoom; only the* x*-cutout is the same. In both cases we have used a filter size of 9 × 9 pixels to estimate the depth and coherence before averaging*

In Figure 3 we show a 80 m × 400 m SAS image. The data was collected in the Oslo fjord, Norway, at approximately 200 m water depth. Figure 4 shows that the seabed is almost completely flat with a 20 cm average depth variation over 400 m ground range. The dominating features are trawl marks, which are estimated to be typically 10–20 cm in depth.

The altitude of the system for this data collection was 42 m, with valid seabed-echo from around one to ten times the altitude, which is equivalent to a change in depression angle ϕ from around 45° to 6° (see Figure 1). Figure 5 shows the estimated average coherence as a function of ground range. As expected from Figure 2, the coherence increases as a function of ground range at short ranges, due to the transmit beampattern. At long ranges, the coherence falls due to transmission loss and lowering of the grazing angle. Notice that we have omitted data where $\phi > 45°$, since these are outside the main lobe of the transmit beam. As we see in Figure 3, there are local variations in the backscattered level due to seabed slope variations. This effect is more evident at long range where the grazing angle is small [18]. This effect gives a variability to the calculated SNR in difference to the modelled SNR in Figure 2.

In Figure 6 we compare the predicted theoretical STD of the depth estimate, found by inserting the estimated coherence into Equations (3) and (4), with the measured STD found using all along-track measurements and a 1 m sliding window in ground range. We see that the estimator does not achieve the lower bound. However, due to the trawl marks, the seabed is non-flat which will increase the STD. Combined with the fact that the curves have the same functional shape and that they differ by a relatively small factor, the performance of our depth estimator can be described by the CRLB, up to a small factor. This is also supported in previous studies [5, 15, 16].

We now evaluate the new adaptive interferometric filter, where the filter size is given by Equation (7). Figure 7 shows the adaptive filter size

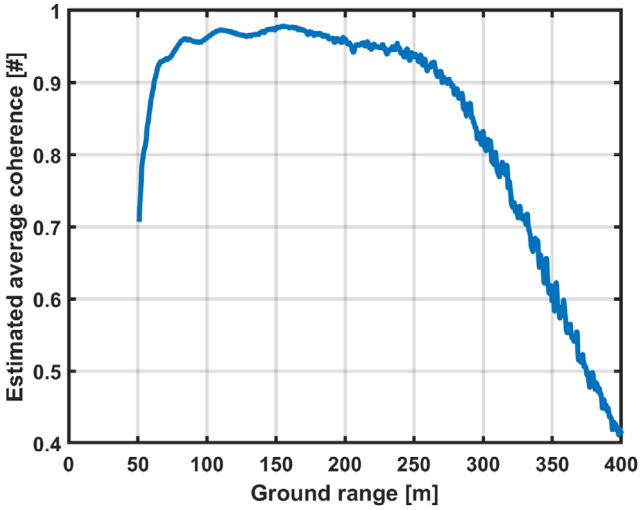

Fig. 5 *Estimated average SAS interferometry coherence using all along-track measurements and a 1 m sliding window in ground range. We have used a filter size of* 9×9 *pixels to estimate the depth and coherence before averaging*

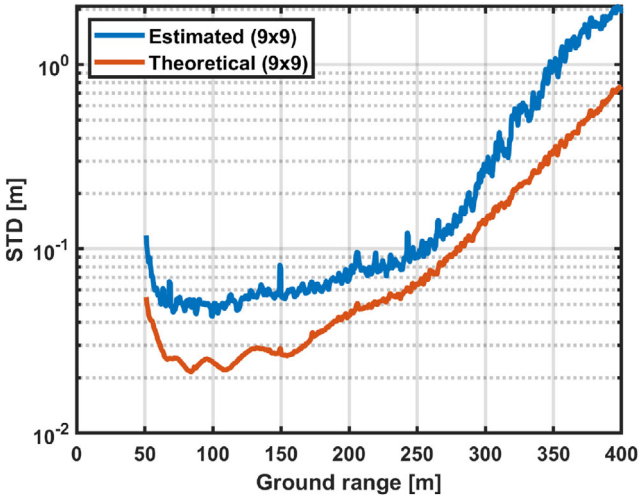

Fig. 6 *Estimated depth STD (blue line) and calculated theoretical STD from the CRLB (red line). The estimates are found by averaging all along-track measurements, and using a 1 m sliding window in ground range. In both cases we have used a filter size of* 9×9 *pixels to estimate the depth and coherence before averaging*

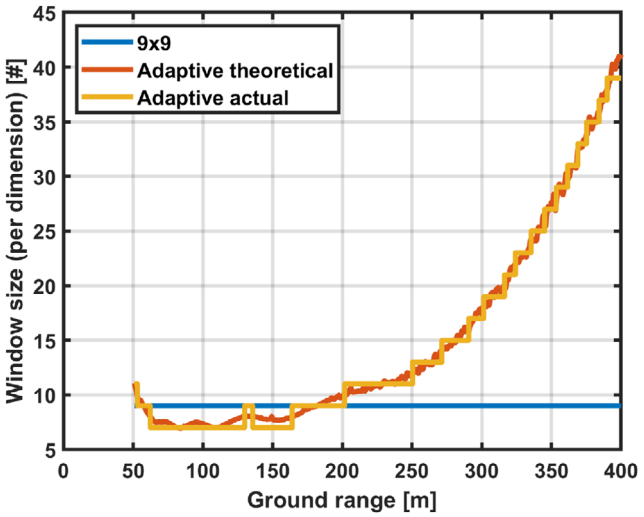

Fig. 7 *Estimated adaptive filter size per dimension,* M*, (red curve), and actual used adaptive filter size restricted to be an odd integer (orange curve). The blue line shows the default filter size* $M = 9$

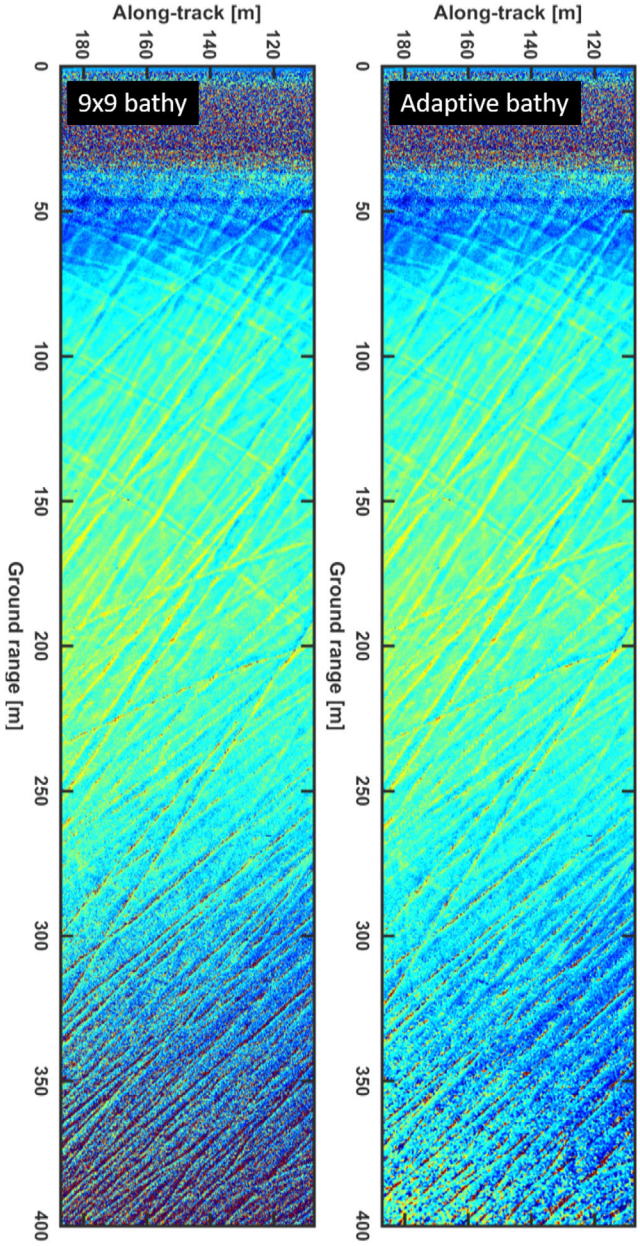

Fig. 8 *Left panel: SAS interferometric depth estimate of a* 80×400 *m flat scene with trawl marks, using default filter size of* 9×9 *pixels. Right panel: Corresponding SAS interferometric depth estimate with adaptive filtering. The dynamic range in both panels is 1 m*

per dimension, M, using the estimated coherence found in Figure 5. For high coherence and relatively short ranges, the adaptive method gives a smaller filter size than the default 9×9 pixels. For longer ranges, the adaptive method gives a significantly larger filter. At 400 m range, the adaptive filter size is 39×39 pixels, which means that a horizontal resolution cell is 78×78 cm. Using $\kappa = 2$, we thus expect the STD of the depth estimate to be 39 cm at 400 m ground range.

Figure 8 shows the measured STD of the estimated bathymetry using the fixed 9×9 filter and the adaptive filter size. We see that using the adaptive filtering, the STD is close to 39 cm at 400 m ground range. The small discrepancy can again be assigned to the fact that the seabed is not completely flat. Figure 8 also shows that the measured STD is equal, or very similar to, the STD using default filtering at short ranges, which is expected, since the filter size is equal, or very similar to, the default 9×9 pixels. For long ranges, our suggested adaptive filtering outperforms the standard method, when it comes to depth STD. If we assume a measurement validity threshold of $\sigma_z = 50$ cm, we see that our adaptive method increases the valid mapping range from 320 m to almost 400 m, at the expense of reduced horizontal resolution.

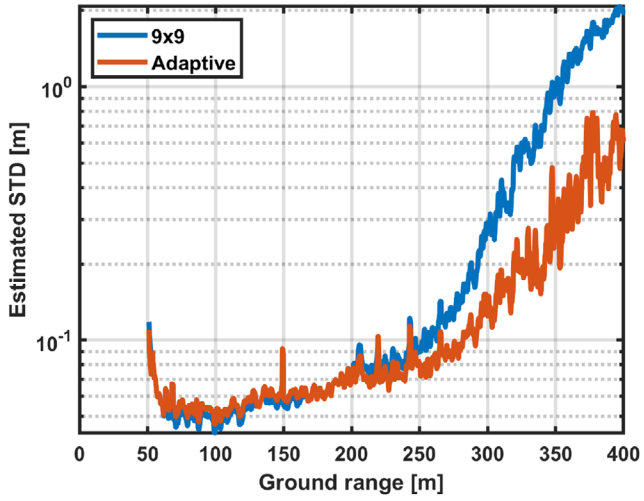

Fig. 9 *Comparison of the estimated depth STD using a default filter size of* 9×9 *pixels (blue line) and an adaptive filter size (red line). The estimates are found by using all along-track measurements and a 1 m sliding window in ground range*

Finally, in Figure 9 we show the estimated bathymetry using default filtering and the estimated bathymetry using adaptive filtering, for the full 80×400 m scene. The dynamic range in the two panels is only 1 m, illustrating that the scene is almost completely flat. The trawl marks are clearly identified throughout the scene, indicating the high resolution and high depth accuracy of SAS interferometry. The colourmap ranges from dark blue to dark red, so the noise-like blue-red pattern at long range for the default 9×9 pixels estimate, indicates the large STD. For the adaptive filtering, the depth estimates are within the 1 m dynamic range almost all the way out to 400 m ground range.

Conclusion: In this paper, we have suggested a novel adaptive filtering in SAS interferometry. Our method adapts the size of the correlation window (or filter) used to estimate the phase difference and the coherence. Since interferometry can be viewed as an estimator of a 3D-position, not only a depth estimator, we suggest an adaptive method, which ensures a pre-defined relation between the horizontal resolutions and the STD of the depth estimates. In practice, our adaptive filter may decrease the size of the correlation window for high SNR and relatively short ranges, which decreases the horizontal resolution at the expense of increased STD of the depth estimates. At long ranges and low grazing angles, where SAS systems usually are noise-limited, our adaptive filter increase the filter size, aiming to keep the STD of the depth estimates at an acceptable level at the expense of reduced horizontal resolution.

We have tested our method on data from a HISAS 1032 Dual receiver sonar. The imaged scene is a 80×400 m flat scene with trawl marks, at around 200 m water depth. For this dataset, our adaptive filtering increases the valid area coverage rate with around 20%, compared to default filtering, at the expense of reduced horizontal resolution at long range. The adaptivity ensures that the horizontal resolution is retained at shorter range, where the SNR is sufficiently high. An alternative method of using a large correlation window at all ranges would have achieved the same STD of the depth estimates, but it would have significantly degraded the horizontal resolution at short ranges.

Acknowledgments: The authors thank Kongsberg Maritime for providing the data used in this study. The authors also thank Darrel Jackson from Applied Physics Laboratory at University of Washington, Seattle, for providing code to produce the sediment backscatter model used in this study. The author finally thanks Anthony Lyons from Center for Coastal and Ocean Mapping/Joint Hydrographic Center at University of New Hampshire for valuable discussions on seabed backscatter.

Conflict of interest: The authors declare no conflict of interest.

Data availability statement: Research data are not shared.

Received: *14 December 2022* Accepted: *26 April 2023*
doi: 10.1049/ell2.12819

References

1 Hayes, M.P., Gough, P.T.: Synthetic aperture sonar: a review of current status. *IEEE J. Oceanic Eng.* **34**(3), 207–224 (2009)
2 Massonnet, D., Souyris, J.C.: *Imaging with Synthetic Aperture Radar. Engineering Sciences*. EFPL Press, Lausanne (2008)
3 Griffiths, H.D., et al.: Interferometric synthetic aperture sonar for high-resolution 3D mapping of the seabed. *IEE Proc. Radar, Sonar Navig.* **144**(2), 96–103 (1997)
4 Hanssen, R.F.: *Radar Interferometry: Data Interpretation and Error Analysis*. Kluwer Academic Publishers, Dordrecht (2001)
5 Sæbø, T.O., Synnes, S.A.V., Hansen, R.E.: Wideband interferometry in synthetic aperture sonar. *IEEE Trans. Geosci. Remote Sens.* **51**(8), 4450–4459 (2013)
6 Sæbø, T.O., Hansen, R.E.: Comparison between interferometric SAS and interferometric SAR. In: Proceedings of Synthetic Aperture Sonar and Radar, Curran Associates, Red Hook, NY (2010)
7 Schmidt, V.E., Weber, T.C., Lurton, X.: Optimizing resolution and uncertainty in bathymetric sonar systems. In: Proceedings of the 1st International Conference and Exhibition on Underwater Acoustics, pp. 1388–1396. Chase Ocean Engineering, Durham (2013)
8 Xu, G., et al.: InSAR phase denoising: a review of current technologies and future directions. *IEEE Geosci. Remote Sens. Mag.* **8**(2), 64–82 (2020). doi:https://doi.org/10.1109/MGRS.2019.2955120
9 Cai, B., Liang, D., Dong, Z.: A new adaptive multiresolution noise-filtering approach for SAR interferometric phase images. *IEEE Geosci. Remote Sens. Lett.* **5**(2), 266–270 (2008). doi:https://doi.org/10.1109/LGRS.2008.915942
10 Hagen, P.E., et al.: Cassandra: an integrated, scalable, SAS based system for acoustic imaging and bathymetry. In: Proceedings of Oceans 2018 MTS/IEEE, pp. 1–6. IEEE, Piscataway, NJ (2018)
11 Richards, M.A.: *Fundamentals of Radar Signal Processing*. 2nd ed. McGraw-Hill Book, New York (2014)
12 Cook, D.A., Brown, D.C.: Synthetic aperture sonar image contrast prediction. *IEEE J. Oceanic Eng.* **43**(2), 523–535 (2018)
13 Richardson, M.D., Jackson, D.R.: The Seafloor. In: Bjørnø, L., Neighbors, T., Bradley, D., (eds.) *Applied Underwater Acoustics*, pp. 469–552. Elsevier, New York (2017)
14 Seymour, M.S., Cumming, I.G.: Maximum likelihood estimation for SAR interferometry. In: Proceedings of IGARSS'94, Vol. **4**, pp. 2272–2275. IEEE, Pisataway, NJ (1994)
15 Sæbø, T.O., Hansen, R.E., Synnes, S.A.V.: Phase ambiguities in synthetic aperture sonar interferometry. In: Proceedings of Oceans 2022 MTS/IEEE. IEEE, Pisataway, NJ (2022)
16 Sæbø, T.O.: *Seafloor Depth Estimation by means of Interferometric Synthetic Aperture Sonar*. University of Tromsø, Tromsø (2010)
17 Touzi, R., et al.: Coherence estimation for SAR imagery. *IEEE Trans. Geosci. Remote Sens.* **37**(1), 135–149 (1999)
18 Lyons, A.P., Olson, D.R., Hansen, R.E.: Modeling the effect of random roughness on synthetic aperture sonar image statistics. *J. Acoust. Soc. Am.* **152**(3), 1363–1374 (2022). doi:https://doi.org/10.1121/10.0013837